8
Thermoelastic Stress Analysis

Janice M. Dulieu-Barton

8.1
Introduction

The purpose of the chapter is to introduce the basics of the full-field, noncontact stress analysis technique known as *thermoelastic stress analysis* (TSA). The technique is based on the measurement of a small temperature change that occurs in an elastic solid as a result of a change in stress or strain. The temperature change is obtained using an infrared detector and is then calibrated in terms of stress. The chapter starts with an introduction to the theory of TSA for isotropic and orthotropic bodies. The basics of infrared thermography as applied to TSA are provided. Following on, the major assumptions in deriving the theory are discussed. The chapter has not been written as a review but as a tutorial for the topic. There are numerous references cited as background throughout the chapter. The chapter ends with an overview of progress and prospects for the future; here some important applications are described and the relevance of the technique to engineering community is demonstrated.

8.2
The Thermoelastic Effect

The relationship between mechanical deformation and thermal energy in an elastic solid is known as the *thermoelastic effect*. The first theoretical treatment of this phenomenon was published for a single material element by Weber and Thomson (Lord Kelvin) as early as 1855. Based on Kelvin's approach, it can be shown that, for a linear elastic homogeneous material, the rate of change of temperature ($\dot{T}$) is a function of the applied deformation in the form

$$\dot{T} = \frac{T_0}{\rho C_\varepsilon}\frac{\partial \sigma_{ij}}{\partial T}\dot{\varepsilon}_{ij} - \frac{\dot{Q}}{\rho C_\varepsilon} \quad \text{for} \quad i, j = 1, 2, 3 \tag{8.1}$$

Optical Methods for Solid Mechanics: A Full-Field Approach, First Edition. Edited by Pramod Rastogi and Erwin Hack.

where T is the temperature, T_0 is the absolute (reference) temperature, C_ε is the specific heat at constant strain, $\dot{Q}$ is the rate of heat loss per unit volume, ρ is the mass density, σ_{ij} is the stress tensor, and $\dot{\varepsilon}_{ij}$ is the rate of change of the strain tensor.

During TSA, the test specimen is dynamically loaded at a frequency high enough so that the heat transfer term ($\dot{Q}$) can be neglected, and hence the relationship given in Eq. (8.1) can be assumed to be adiabatic. The minimum frequency required is dependent on the thermal conductivity of the test material and stress gradients in the structure and is discussed in detail in a following section.

To develop Eq. (8.1) into a simple equation that can be applied experimentally, it is necessary to express the stresses in terms of strains and temperature to obtain the derivative $\partial\sigma_{ij}/\partial T$. For an isotropic, linear elastic material, the constitutive stress–strain–temperature relationships can be expressed in terms of the Lamé constants in the form

$$\sigma_{ij} = 2\mu\varepsilon_{ij} + (\lambda\varepsilon_{kk} - \beta\delta T)\delta_{ij} \tag{8.2}$$

for

$$\delta_{ij} = \begin{cases} 1 & \text{for} \quad i = j \\ 1 & \text{for} \quad i \neq j \end{cases}$$

and

$$\beta = (3\lambda + 2\mu)\alpha$$

where ε_{kk} is the first strain invariant (i.e., $\varepsilon_{11} + \varepsilon_{22} + \varepsilon_{33}$), δT is the change in temperature ($\delta T = T - T_0$), and α is the coefficient of linear thermal expansion. The Lamé constants λ and μ are functions of the Young's Modulus E and Poisson's ratio ν, as follows:

$$\mu = \frac{E}{2(1+\nu)}$$

and

$$\lambda = \frac{\nu E}{(1+\nu)(1-2\nu)} \tag{8.3}$$

The derivatives of stress with respect to T are obtained from Eq. (8.2) as follows:

$$\frac{\partial\sigma_{ij}}{\partial T} = 2\frac{\partial\mu}{\partial T}\varepsilon_{ij} + \left(\frac{\partial\lambda}{\partial T}\varepsilon_{kk} - \frac{\partial\beta}{\partial T}\delta T - \beta\right)\delta_{ij} \tag{8.4}$$

Equation (8.4) contains the *temperature derivatives of the material elastic properties*. For most engineering materials, the variations of the elastic properties with temperature are practically zero at room temperature, so in this treatment they are neglected. (The consequences of making this assumption are described in Section 8.9.) For a stress-induced temperature field, δT is in the order of millikelvin and therefore the

) temperature, C_ε is the
ss per unit volume, ρ is
e of change of the strain

ed at a frequency high
eglected, and hence the
diabatic. The minimum
tivity of the test material
in detail in a following

applied experimentally, it
nd temperature to obtain
material, the constitutive
ed in terms of the Lamé

(8.2)

ε_{33}), δT is the change in
linear thermal expansion.
s Modulus E and Poisson's

(8.3)

from Eq. (8.2) as follows:

(8.4)

mate... elastic properties. For
properties with temperature
eatment they are neglected.
scribed in Section 8.9.) For a
millikelvin and therefore the

term $(\partial\beta/\partial T)\delta T$ will be negligible compared to β, so this term is also neglected to give a simplified version of Eq. (8.4) as

$$\frac{\partial \sigma_{ij}}{\partial T} = -\beta \delta_{ij} \tag{8.5}$$

Substituting Eq. (8.5) into Eq. (8.1), and assuming *adiabatic conditions*, where $\dot{Q} = 0$, gives an expression for the rate of temperature change in terms of the material properties and the applied deformation, which can be written as

$$\dot{T} = -\frac{T_0 \beta}{\rho C_\varepsilon} \dot{\varepsilon}_{kk} \tag{8.6}$$

Expressing $\dot{\varepsilon}_{kk}$ in terms of stress using the relationship given in Eq. (8.2) yields

$$\dot{T} = -\alpha \left[\frac{T_0}{\rho C_\varepsilon} + \frac{1 - 2\nu}{3\alpha^2 E} \right] \dot{\sigma}_{kk} \tag{8.7}$$

where $\dot{\sigma}_{kk}$ is the rate of change of the sum of the first stress invariant $(\sigma_{11} + \sigma_{22} + \sigma_{33})$.

The bracketed term in Eq. (8.7) comprises mainly material constants. However, T_0 may vary from test to test and it would be convenient to express Eq. (8.7) as a linear function of the material properties. To do this, C_ε can be expressed in terms of the specific heat at constant pressure (C_p) using the relationship

$$C_\varepsilon = C_p - \frac{3E\alpha^2 T_0}{\rho(1 - 2\nu)} \tag{8.8}$$

Therefore, Eq. (8.7) can be rewritten as

$$\dot{T} = -\frac{\alpha T_0}{\rho C_p} \dot{\sigma}_{kk} \tag{8.9}$$

Equation (8.9) directly relates the rate of change of temperature to the rate of change of stress in the specimen. Integrating this expression over a time period from the initial state to the final state of deformation provides a linear relationship between the change in temperature (ΔT) and the change in the first stress invariant $(\Delta\sigma_{kk})$ in the form

$$\Delta T = -K T_0 \Delta \sigma_{kk} \tag{8.10}$$

where K is known as the *thermoelastic constant* and is a function of the material properties as follows:

$$K = \frac{\alpha}{\rho C_p} \tag{8.11}$$

to yield the more familiar form of

$$\Delta T = -\frac{\alpha T_0}{\rho C_p} \Delta(\sigma_1 + \sigma_2) \tag{8.12}$$

Equation (8.12) is the standard form of the thermoelastic equation for an isotropic, homogeneous material loaded elastically, where it is assumed that the temperature change occurs adiabatically.

Tutorial Exercise 8.1

An image is obtained from an aluminum alloy aircraft structure during testing where the ambient temperature is measured as 27 °C. The aluminum alloy is reported to have a coefficient of thermal expansion of $23.5 \times 10^{-6}\ K^{-1}$, a density of $2700\ kg\ m^{-3}$, and a specific heat at constant pressure of $900\ J\ kg^{-1}\ K^{-1}$. During a tensile test, the yield strength of the aluminum alloy was determined as 110 MPa and Young's modulus of 68 MPa. In the image the maximum ΔT value is 0.377 K. Discuss the implications of this finding on the integrity of the component.

Solution:

From Eqs. (8.11) and (8.12)

$$K = \frac{\alpha}{\rho C_p} = \frac{23.5 \times 10^{-6}}{2700 \times 900} = 9.67 \times 10^{-6}\ MPa^{-1}$$

Neglecting the negative sign in Eq. (8.12) (see Section 8.7 for explanation),

$$\frac{\Delta T}{KT} = \Delta\left(\alpha_1 + \alpha_2\right) = \frac{0.377}{9.67 \times 10^{-6} \times 300} = 130\ MPa$$

$\Delta(\alpha_1 + \alpha_2)$ is in excess of the yield stress of the material. However, this does not indicate that the component will yield, as the quantity is the sum of the principal stresses. If $\sigma_1 = \sigma_2$, then neither of the principal stresses is above the yield stress. If one of the principal stresses is negative, then this means that either may be above yield. The conclusion is that further investigation is required either by attaching a strain gauge rosette or by modeling. It should be noted that the negative sign in Eq. (8.12) has been ignored. This is because the phase of the response is set 180° out of phase to make a tension give a positive ΔT.

8.3 Infrared Thermography

A body with a temperature above absolute zero will emit energy in the form of electromagnetic radiation/thermal radiation at its surface. As the temperature increases, the quantity of heat transferred by means of thermal radiation increases. By using the amount of energy emitted in the form of electromagnetic radiation, accurate temperature measurements can be made over a wide range by means of infrared thermography. The spectral radiant emittance ($\Phi_{\lambda,b}$) for a blackbody in a hemisphere in the wavelength range from λ to $\lambda + \delta\lambda$ can be found using *Planck's law* [2], that is,

$$\Phi_{\lambda,b} = \frac{C_1}{\lambda^5\left(\exp^{C_2/\lambda T} - 1\right)} \tag{8.13}$$

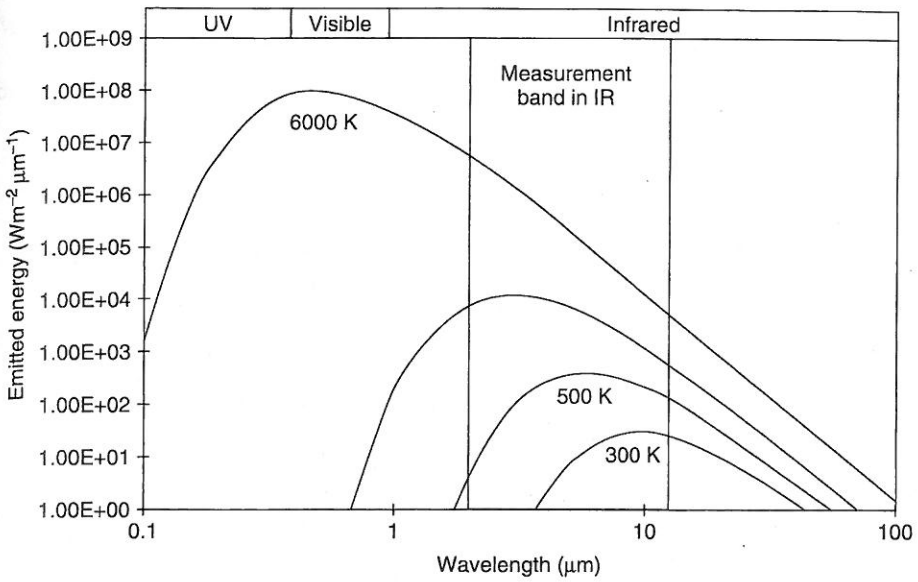

Figure 8.1 Radiant emitted energy from a blackbody according to Planck's law.

where C_1 is the first radiation constant $= 2\pi c^2 h$ (h is Planck's constant, c is the speed of light, and λ is wavelength), C_2 is the second radiation constant $= ch/k$ (k is the Boltzmann constant), and T is the absolute temperature.

The spectral radiant emittance for a blackbody at various temperatures can be plotted against wavelength as shown in Figure 8.1. It is possible to detect the radiant emittance by using an infrared detector. These are basically electronic devices that are sensitive to photon emission in the infrared spectrum, which has a peak between 2 and 12 μm at ambient temperature as shown in Figure 8.1. In modern infrared detection systems, the detector is built into a camera system with a lens and electronics, which enables the camera to have a computer interface. Low-sensitivity detectors are usually bolometers; higher sensitivity devices are usually *photon detectors* and these are used for strain measurement. The intensity of the photon collection defines the electrical signal output from the detector as the detector acts as a transducer turning a photon strike into a voltage signal.

By integrating Planck's law (Eq. (8.13)) over all wavelengths between zero and infinity, it is possible to obtain a finite integral and obtain the well-known fourth-power *Stefan–Boltzmann* relationship for evaluating the radiant emittance Φ_b as follows:

$$\Phi_b = 2\pi c^2 h \int_0^\infty \frac{d\lambda}{\lambda^5 \left(\exp\left(ch/kT\lambda\right) - 1\right)} \tag{8.14}$$

Letting $x = ch/kT\lambda$ allows the integration to be processed by substitution with respect to x. Thus, x must be rewritten to make λ the subject and subsequently

differentiated with respect to x. That is: $\lambda = ch/kTx$, $d\lambda/dx = ch/kTx^2$, and $\lambda^5 = (c^5h^5)/(k^5T^5x^5)$.

Substituting the relationship for λ^5 and the derivative of λ with respect to x into Eq. (8.14) leaves

$$\Phi_b = \frac{2\pi c^3h^2k^5T^5}{c^5h^5kT}\int_0^\infty \frac{x^5\,dx}{x^2\left(\exp\left(ch/kT\lambda\right)-1\right)} \tag{8.15}$$

and Eq. (8.15) can be simplified to

$$\Phi_b = \frac{2\pi k^4T^4}{c^2h^3}\int_0^\infty \frac{x^3\,dx}{\exp(x)-1} \tag{8.16}$$

Using the integral in Eq. (8.16), the radiant emittance can be written as follows:

$$\Phi_b = \left(\frac{2\pi^5k^4}{15c^2h^3}\right)T^4 \tag{8.17}$$

This result can be simplified by rewriting the right-hand side of Eq. (8.20) through the introduction of the *Stefan–Boltzmann* constant B as the bracketed term to give the fourth-power *Stefan–Boltzmann* relationship for evaluating the radiant emittance over all wavelengths λ_b as follows:

$$\Phi_{\lambda,b} = BT^4 \tag{8.18}$$

It can be shown that $\Phi_{\lambda,b}$ has a maximum. The wavelength at which this occurs is defined as λ_{max}, and can be calculated from *Wien's displacement law* [2].

In a similar manner, it is possible to obtain a discrete equation for the number of photons (N_b) emitted by an object at a specific temperature by dividing the energy in each wavelength interval by the energy carried by each photon. To evaluate the relationship for a general case, the photon flux can be derived for the total number of photons per unit area and time by producing a closed-form integral of the equation for spectral radiant emittance; again, this is only possible by considering the wavelength range between zero and infinity, as

$$N_b = \int_0^\infty \frac{2\pi c}{\lambda^4\left(\exp\left(hc/\lambda kT\right)-1\right)}\,d\lambda \tag{8.19}$$

The integration is possible using the substitution method and the subsequent derivatives presented for Eq. (8.15). Noting that here λ is raised to the power 4, in this case the λ terms can be rewritten for this derivation as

$$\lambda^4 = \frac{c^4h^4}{k^4T^4x^4} \tag{8.20}$$

Substituting into Eq. (8.19) leaves

$$N_b = \frac{2\pi ck^4T^4}{c^4h^4}\frac{ch}{kT}\int_0^\infty \frac{x^4}{x^2(\exp((x)-1)}dx \tag{8.21}$$

$\mathrm{d}\lambda/\mathrm{d}x = ch/kTx^2$, and

f λ with respect to x into

(8.15)

(8.16)

ı be written as follows:

(8.17)

side of Eq. (8.20) through
as the bracketed term to
or evaluating the radiant

(8.18)

gth at which this occurs is
cement law [2].
quation for the number of
ure by dividing the energy
h photon. To evaluate the
rived for the total number
osed-form integral of the
ly possible by considering

(8.19)

ethod and the subsequent
is raised to the power 4, in
ı as

(8.20)

(8.21)

which again can be simplified as

$$N_b = \frac{2\pi k^3 T^3}{c^2 h^3} \int_0^\infty \frac{x^2\,\mathrm{d}x}{\exp(x) - 1} \tag{8.22}$$

The integral in Eq. (8.22) may be evaluated in a similar manner to that used previously to give

$$N_b = \frac{2\pi k^3 T^3}{c^2 h^3}(2.4041) \tag{8.23}$$

This formulation again allows the substitution of the *Stefan–Boltzmann* constant to provide the following relationship between the number of photons incident and the surface temperature:

$$N_b = \frac{0.370B}{k} T^3 \tag{8.24}$$

The quantity $0.370B/k = 1.52 \times 10^{15}$ photons $\mathrm{s}^{-1}\ \mathrm{m}^{-3}\ \mathrm{sr}^{-1}\ \mathrm{K}^{-3}$ can be regarded as the *Stefan–Boltzmann constant for photodetectors*. Denoting the constant for photodetectors as B', Eq. (8.24) simplifies to

$$N_b = B'T^3 \tag{8.25}$$

The relationship presented in Eq. (8.25) shows that, when considering the entire electromagnetic spectrum, the total number of photons increases with the cube of the absolute temperature, whereas the radiant emittance over the entire spectrum increases with the fourth-power of absolute temperature. The relationship for the number of photons (N_b) emitted from a surface as derived above and presented in Eq. (8.25) has been used to relate the photon output from an infrared detector to the temperature, but these should be regarded as an approximation. For infrared thermography, there are two atmospheric windows of interest: one is located from 3 to 5 μm (most bolometers and photodetectors) and the other is from 8 to 12 μm (some photodetectors). The number of photons per unit area and time is obtained by integrating the spectral photon emittance over the operating wavelength band of the photodetector instead of the range $0 - \infty$. It is impossible to derive a closed-form relationship, as presented for the radiant emittance or photon flux above, for practical narrow-band IR detectors. Therefore, it is necessary to consider other mathematical methods to express the relationship between the spectral radiant power and the absolute temperature between the wavelength limits of the infrared detectors of interest. Clearly, this will not yield the same result given by the formulation of Eq. (8.25). For detectors where the operating wavelength is much less than λ_{max}, then the response of the detector to temperature changes follows an approximate power law, that is, $N_b \propto T^n$ [3]. Therefore, it is possible to propose an expression that relates the surface temperature of a body to the total number of photons emitted over a particular wavelength range as follows:

$$N_{b_\lambda} = B'T^n \tag{8.26}$$

where B' is a constant that is dependent on the detector. The index n can be evaluated by determining N_{b_λ} from Eq. (8.19) by numerical integration over the

wavelength of interest for a variety of temperatures. Taking logs of Eq. (8.26) will yield a simple linear form, that is,

$$\ln N_{b_\lambda} = \ln B' + n \ln T \tag{8.27}$$

where n can be determined from the slope of a plot of $1nN_{b_\lambda}$ against $\ln T$ and B can be derived from the intercept of the plot. Equation (8.30) can be used as a basis for calibration; however, most instruments are supplied with empirical calibration curves from the manufacturer.

When radiation impinges on a body, it is either transmitted through the body, absorbed by the body, or reflected away from the body, so that

$$\tau + a + r = 1 \tag{8.28}$$

where τ is the transmissibility, a is the absorptivity, and r is the reflectivity.

Engineering materials are usually opaque in the infrared region, even if they are transparent to visible light, for example, glass. The transmitted energy is therefore zero. So Eq. (8.28) can be rewritten as

$$a + r = 1 \tag{8.29}$$

The reflectivity is then $1 - a$, so a portion of incident radiation is reflected back to the detector. Care must be taken to avoid anomalous readings from reflections from heat sources. The absorbed energy is therefore equal to the emitted energy, and so

$$a = e \tag{8.30}$$

where e is the emissivity.

The variability in emissivity means that care is required to interpret the measured temperature and to take account of background radiation. Often, a layer of matt black paint is applied to the surface of a material to create an enhanced and uniform emissivity. It is interesting that this is not usually necessary for polymeric materials. Infrared systems are usually calibrated using a blackbody; therefore, it is necessary to input a surface emissivity before calibrating the response into a temperature value.

8.4 Obtaining Thermoelastic Measurements from an Infrared System

In early work, the total radiant flux emitted from a surface was used to develop a working relationship for thermoelastic studies [4]. It follows by differentiation of the standard Stefan–Boltzmann relationship that the flux change $\Delta\Phi$ resulting from a small change in the surface temperature ΔT is given by

$$\Delta\Phi = 4eBT^3\Delta T \tag{8.31}$$

The surface emissivity e is included, which is important to consider in TSA, as it is probable that the surface will not behave like a blackbody.

If the flux change is recorded by a linear detecting system, the detector voltage output (S) will be proportional to the change in temperature, and therefore it follows from Eq. (8.31) that the change in the principal material stresses is given by

$$S = -\frac{4R^* eB\rho C_p T^4}{\alpha}(\Delta\sigma_1 + \Delta\sigma_2) \tag{8.32}$$

where R^* is some detector response factor for the system.

Grouping the variables before the bracket on the right-hand side of Eq. (8.32) as those dependent on the material under test and the settings of the detector system, a calibration constant A is defined. The general thermoelastic relationship is therefore as follows [4]:

$$AS = (\Delta\sigma_1 + \Delta\sigma_2) \tag{8.33}$$

This treatment neatly obviates the inaccuracies associated with using the simple Stefan–Boltzmann relationship. However, the calibration constant has to be defined for every surface temperature, as there is a very strong detector dependence on surface temperature particularly for the detectors that operate on the 2–5 μm wavelength range. Equation (8.33) has been used as the basis for numerous studies spanning almost three decades. Since the initial validation in [4], it has been demonstrated that the approach can be used in a wide range of applications; some example applications are provided throughout the chapter, particularly in the final section.

Orthotropic Materials

The simple thermoelastic theory devised for an isotropic body in Eq. (8.36) is not valid for orthotropic materials [5]. For orthotropic materials, the following equation is used [5]:

$$(\alpha_1\Delta\sigma_1 + \alpha_2\Delta\sigma_2) = A^*S \tag{8.34}$$

where $\Delta\sigma$ is the change in the direct surface stress, A^* is a further calibration constant, and the subscripts 1 and 2 denote the principal material directions of the surface lamina.

Stanley and Chan [5] validated Eq. (8.34) using two types of composite component. Potter [6] proposed a thermoelastic theory relating the thermoelastic output to that of the surface strains and demonstrated its validity on a carbon fiber/epoxy resin laminate. Bakis and Reifsnider [7] investigated the influence of material inhomogeneity and anisotropy using carbon-fiber-reinforced plastics. It was found that the thermoelastic response was affected by a number of factors, which included the volume fraction, the thermoelastic properties of the microconstituent materials, the orientations of the laminae within the laminate, and the orientation of the lamina on the surface.

8.5
Temperature Dependence of Thermoelastic Response

To derive a surface temperature correction factor that could be realistically inserted into Eqs. (8.33) and (8.34), an expression that is just a function of temperature is desirable. An approximate approach has been suggested [8] for detectors where the operating wavelength is less than λ_{max}. Here, the response of the detector to temperature changes follows an approximate power law, that is, $N_b \propto T^n$. Equations (8.26) and (8.27) can be used to provide a relationship [8] for the surface temperature of a body to the total number of photons emitted over a particular wavelength range. Equation (8.27) shows that the index n and B' can be obtained from a log–log plot of $\ln N_{b_\lambda}$ against $\ln T$; B can be derived from the intercept of the plot.

For a specimen with an absolute temperature of 293 K, λ_{max} occurs at 9.89 μm. Therefore, as the power law is valid only for cases where the operating wavelength of the detector is less than λ_{max}, at around room temperature the relationship given by Eq. (8.26) is valid for the 2–5 μm range but not in the 8–12 μm range. A numerical integration of Planck's law over the 2–5 μm range for temperatures of 293–323 K using MATLAB and application of the above procedure [8] yielded $B = 6.322 \times 10^6$ photons s^{-1} m^{-3} sr^{-1} $K^{-10.47}$ and $n = 10.47$; the correlation coefficient for the curve fit was 0.99. Therefore, a temperature correction factor can be introduced as $(T_0/T)^{10.47}$. There is a huge difference between the standard approach using the photon detector law and calculating over the correct wavelength range. Hence Eqs. (8.33) and (8.34) should be used with caution. In view of this, it is much better to have an empirical radiometric calibration against a blackbody and apply Eq. (8.10) directly. The validations carried out in [5] used a detector that worked in the 8–12 μm range. Here, the temperature sensitivity is less and the temperature correction follows approximately a cube law.

8.6
Derivation of the Thermoelastic Constant

Until recently, the approach in TSA was to derive the calibration factor (A in Eq. (8.33)). The three principal calibration techniques used to derive a value for A, are as follows [9]:

1) Direct calibration, using properties of the infrared detector, system variables, specimen surface emissivity, and the thermoelastic constant of the specimen material;
2) Calibration against measured stress;
3) Calibration against calculated stress.

The direct calibration (method (1)) is based on solving Eq. (8.32) and utilizes both material and detector properties to theoretically derive a value for A. This method is not regarded as the most accurate. The second method utilizes an independent measure of strain (typically an electrical resistance strain gauge). The sum of the

principal stresses can be determined using the strain measurements and Hooke's law; however, values for the material's Young's modulus and Poisson's ratio are required. The third technique used for calibration requires a known stress field. Normally, a specimen constructed from the material in question is loaded in simple tension. (A beam in four-point bending and a disc in two-point diametral compression are other recommended arrangements.) The stress can be calculated theoretically using the cross-sectional area and the applied load. Equation (8.33) is simplified to find a value for A. This method has the least potential for error sources. Techniques based on these calibration approaches are currently being developed into a standard for TSA measurements [10].

Identical approaches can be used to find the thermoelastic constant K. Here, Eq. (8.12) is used, and a known stress is applied to a specimen; ΔT and T are obtained from the measurement and therefore K is obtained.

Tutorial Exercise 8.2

An independent verification of the thermoelastic constant K of the aluminum alloy used in Tutorial Exercise 8.1 is required. This is to be done with a strip of the alloy 15 mm wide by 5 mm thick loaded in uniaxial cyclic tension with a load cycle of 4 ±2.5 kN at 10 Hz. During the test, room temperature is measured as 21 °C and the average ΔT values over the uniform area of the strip is obtained at 0.180 ±0.005 K. Derive the value of K and discuss this in the context of the value of K obtained in Tutorial Exercise 8.1.

Solution:

For an uniaxial test, the stress is obtained from the force and geometrical values:

$$\Delta\sigma_1 = \frac{5 \times 10^3}{15 \times 5} = 66.7 \text{ MPa}$$

$$K = \frac{\Delta T}{T\Delta(\sigma_1 + \sigma_2)} = \frac{0.180}{294 \times 66.7} = 9.20 \times 10^{-6} \text{ MPa}^{-1}$$

The K value obtained from the experiment is 5% less than that calculated from the literature. This is typical, as the exact grade of aluminum alloy is not known and even so properties vary with the grade. It is essential that a calibration test piece is made from the same billet of aluminum alloy from the same rolling direction.

A number of quantitative studies have been carried out on orthotropic composite structures, for example, by deriving a calibration constant [11–13]. A generalized calibration routine was suggested in [14] but has not been fully developed. The routine was based on the response from the resin-rich surface layer and assumes that the response is that of the resin alone acting as strain witness. This may only be true for certain material combinations but has also been observed by other researchers [15, 16]. A general conclusion is that it is not possible at present to apply TSA in a straightforward manner to a general composite structure and obtain quantitative stress or strain values.

8.7 Nonadiabatic Conditions

Nonadiabatic conditions exist when the rate of heat flux per unit volume ($\dot{Q}$) is different from zero. It is impossible to achieve fully adiabatic conditions experimentally; however, for the purposes of TSA a *pseudo-adiabatic* state may be achieved, where there is no measurable attenuation of the thermoelastic signal because of heat transfer. To understand the limitations of the pseudo-adiabatic assumption, it is useful to use the following expression:

$$\dot{T} = -\frac{\alpha T_0}{\rho C_p}\dot{\sigma}_{kk} - \frac{\dot{Q}}{\rho C_\varepsilon} \tag{8.35}$$

The magnitude of $\dot{\sigma}_{kk}$ can be amplified by increasing the loading frequency and thereby making it much greater than the $\dot{Q}$ term. This is usually the approach taken to obtain a pseudo-adiabatic state, with a loading frequency of 10–20 Hz being sufficient for most applications.

$\dot{Q}$ is a function of the thermal conductivity of the material and the stress-induced thermal gradients in the component, and can be expressed in the form

$$\dot{Q} = k\nabla^2 T \tag{8.36}$$

where k is the material thermal conductivity and $\nabla^2 T$ is the thermal flux defined as

$$\nabla^2 T = \frac{\partial^2 T}{\partial x^2} + \frac{\partial^2 T}{\partial y^2} + \frac{\partial^2 T}{\partial z^2} \tag{8.37}$$

Analysis of Eq. (8.35) shows that, for a specimen with a uniform stress field or a low k value, the $\dot{Q}$ term will be small. In both cases, a pseudo-adiabatic state is achieved at low loading frequencies. However, most engineering components have stress gradients and are made from metals that have a high thermal conductivity.

Finite element analysis (FEA) may be used to analyze nonadiabatic affects at loading frequencies that cannot be achieved experimentally. It may be used to determine the loading frequency where $\dot{Q}$ can be neglected for a given stress field and a given set of material properties. In close proximity of stress raisers, attenuation of the thermoelastic signal is an important consideration, even at loading frequencies of 20 Hz and above. Often, the attenuation effects are localized and TSA can still be used to obtain quantitative data from most specimens. This is verified by the large number of publications that have successfully used TSA to obtain quantitative data at loading frequencies less than 15 Hz.

Nonadiabatic behavior can be investigated experimentally by examining the thermoelastic response over a range of frequencies. If the response is independent of frequency, it can be assumed that a pseudo-adiabatic state has been achieved. Furthermore, it is possible with the lock-in thermography system required for TSA not only to obtain the magnitude of the thermoelastic response but also its phase relative to the applied cyclic load. As a positive stress change results in a decrease

in response (i.e., a cooling analogous to the expansion of a gas and denoted by the minus sign in Eq. (8.12)), the stress change is always 180° out of phase with the temperature change. However, in standard practice the measurement system is usually set so that a tensile stress change is in phase with the temperature change and hence the minus sign in Eq. (8.12) is often neglected. The phase provides a convenient tool for assessing nonadiabatic behavior, as any phase lead or lag indicates that the stress change is not in phase with the temperature change and Eq. (8.12) is not valid. Heat conduction in areas of high stress gradient causes changes in the magnitude of the thermoelastic response as well as a phase shift. Discontinuities in the phase image can be used to identify nonadiabatic regions in a specimen. This is evident in Figure 8.2, which shows the magnitude and phase images from a strip of material loaded in uniaxial tension. Here, the area above and below the hole, which are in compression, are out of phase with the rest of the plate. Moreover, close to edge of the hole (right and left in the image), areas of out-of-phase signal are apparent, where the stress gradient is the greatest.

The resolution of the detection system is also a consideration when obtaining pseudo-adiabatic conditions. TSA of small-scale structures requires a detection system with a high spatial resolution to ensure that an adequate number of measurements are obtained across the structure to build an accurate representation of the signal distribution. However, at high resolutions each detector element is projected over a very small area on the test specimen. The average temperature in the projected area is used to derive the thermoelastic signal. The smaller the measurement area, the greater effect the $\dot{Q}$ term on the thermoelastic measurements. At high detector resolutions, acute stress gradients are not averaged out over large measurement areas and therefore the sensitivity of the signal to nonadiabatic effects is increased. A treatment for establishing whether the response is adiabatic has recently been proposed [17]. Here, small discs were examined, and it was shown that by using a combination of the thermal diffusion properties and the specimen geometry a procedure could be applied to identify whether adiabatic conditions had been achieved.

Bakis and Reifsnider [7] investigated the limitations of Eq. (8.34) in terms of the adiabatic thermoelastic assumption made in its development. For composite materials, it was suggested that the nonadiabatic behavior in carbon-fiber-reinforced plastic (CFRP) laminates could be due to heat transfer between the fiber and matrix or caused by viscoelastic effects. The former was discounted [19] for fibers of diameter $\approx 7\ \mu m$, which is typical for carbon fibers. Wong *et al.* [19] discussed the effects of nonadiabatic conditions on the thermoelastic signal recorded from the specimen surface due to heat transfer characteristics at large stress gradients, such as those experienced between plies orientated at different angles in a laminate.

TSA is widely considered as a technique for establishing surface strains or stresses. However, it was suggested in [20] that the nonadiabatic response could be used to establish subsurface stresses. Some initial work on identifying subsurface damage is described in [21], which demonstrates the potential of the technique for materials with high thermal conductivities.

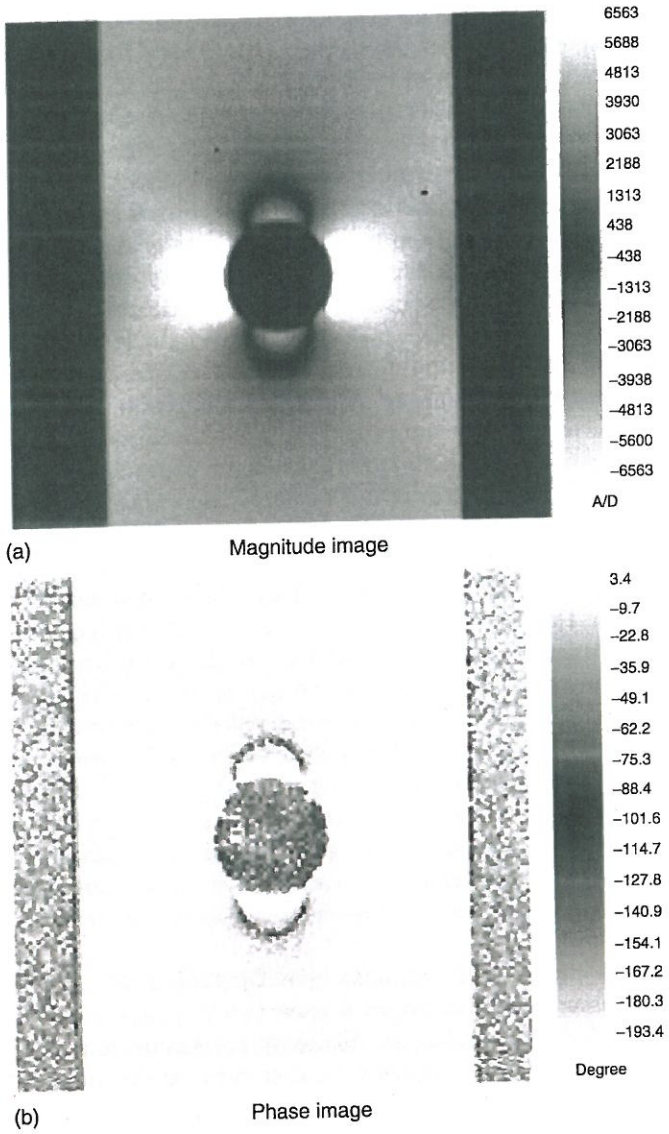

Figure 8.2 TSA data from hole in a plate specimen. (Please find a color version of this figure on the color plates.)

8.8 Paint Coatings

It is a standard practice when taking thermographic measurements to coat the specimen surface with a thin layer of matt black paint to improve emissivity and ensure that the response is uniform. However, this coating is thermally inert in comparison with the specimen and may, in certain instances, give rise to

nonadiabatic effects. Thermal lag [22] is caused by the insulating effect of the paint coating. Even with no heat loss to the environment, a surface coating will still have a capacitance and resistance associated with it, which will result in a temperature drop across it. In short, an increase in paint coating thickness will result in a smaller ΔT at the paint surface than at the substrate surface. This is significant for small-scale specimens where it can be difficult to apply an even paint coating, especially in areas where there are sharp changes in section. In general, most practitioners will recommend a minimal amount of paint [23]. Two short passes of paint supplied using an aerosol is deemed suitable for most applications.

Thermal drag-down [22] is a phenomenon relating to both the paint thickness and the loading frequency. Since no heat is being generated by the coating, its temperature can only change because of the heat transferred to it from the substrate. As the loading frequency increases, the spatial wavelength decreases; as a result, there is less heat input into the coating. In brief, the heat will not flow into the surface coating sufficiently quickly to maintain the temperature change for accurate thermoelastic measurements to be recorded.

A theoretical treatment for covering the effects of paint coating has been developed [24], where four distinct regions of coating response were identified:

- *High-emissivity coating region*, where the temperature change on the surface of the coating is identical to that on the surface of the material;
- *Opacity-limited region*, where the coating is so thin that the surface emissivity is a combination of the paint coating and the specimen surface;
- *Coating diagnostic region*, where thermal drag-down is experienced as the loading frequency is increased;
- *Strain witness region*, where the coating is so thick, or loading frequency so high, that the thermoelastic response is from the coating alone.

A detailed experimental study of the effect of paint coating on a variety of materials is provided in [25]. A typical plot showing contours of ΔT for changing frequency and paint thickness is shown in Figure 8.3. Here, it can be seen clearly that the desirable high-emissivity region occurs to the top left of the plot and it is likely, except for very thin coatings, that the measurements will be taken in the coating diagnostic region where the response is dependent on frequency because of thermal dragdown.

8.9 Temperature Dependence of the Material Elastic Properties

For the small changes in temperatures associated with the thermoelastic effect, the thermoelastic constant K is assumed to be a material constant that is independent of the stress field. However, K is a function of the coefficient of linear expansion α, which has been shown to be stress dependent as follows:

$$\left(\frac{\partial \alpha}{\partial \sigma}\right)_T = \frac{\partial}{\partial \sigma}\left[\left(\frac{\partial \varepsilon}{\partial T}\right)_\sigma\right]_T = \frac{\partial}{\partial T}\left[\left(\frac{\partial \varepsilon}{\partial \sigma}\right)_T\right]_\sigma \tag{8.38}$$

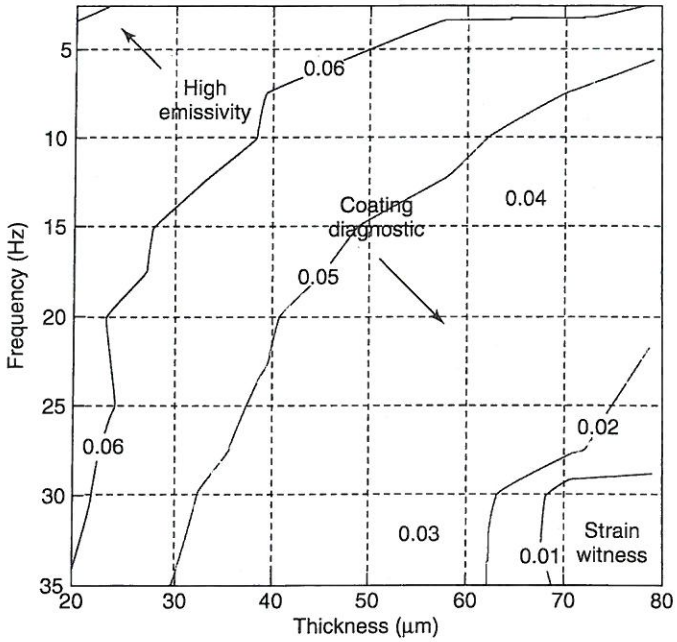

Figure 8.3 Contour plot of experimental response with changing frequency (2.5–35 Hz) and paint thickness (20–80 μm).

Therefore, if $E = (\partial\sigma/\partial\varepsilon)_T$, differentiating by parts gives

$$\left(\frac{\partial\alpha}{\partial\sigma}\right)_T = -\frac{1}{E^2}\left(\frac{\partial E}{\partial T}\right)_\sigma \tag{8.39}$$

Equation (8.39) shows that α will be stress dependent for materials whose elastic properties are sensitive to changes in temperature. This also implies that the thermoelastic response of such materials will be dependent on the mean stress of the applied stress cycle and cannot be assumed to be constant.

The theoretical approach presented previously assumes that the dependence is a higher order effect and can be neglected for most engineering materials. Although this hypothesis has been shown to be valid for most applications, it may not be valid for some materials, particularly those with high-temperature sensitivity used in components where a high mean stress is applied, in which case the following equation must be used [26]:

$$\dot{T} = \frac{T_0}{\rho C_\varepsilon}\left[\left(-\beta - \frac{\partial\beta}{\partial T}\delta T + \frac{\partial\lambda}{\partial T}\varepsilon_{kk}\right)\delta_{ij} + 2\frac{\partial\mu}{\partial T}\varepsilon_{ij}\right]\dot{\varepsilon}_{ij} - \frac{\dot{Q}}{\rho C_\varepsilon} \tag{8.40}$$

The $(\partial\beta/\partial T)\delta T$ term will be negligible compared to β and can be neglected. However, for some materials the terms $(\partial u/\partial T)\varepsilon_{ij}$ and $(\partial\lambda/\partial T)\varepsilon_{kk}$ can be of a

significant order. Therefore, retaining these terms and omitting higher order components allows Eq. (8.42) to be written in terms of stresses for adiabatic conditions as follows:

$$\dot{T} = \frac{T_0}{\rho C_p}\left\{-\left(\alpha + \left(\frac{\nu}{E^2}\frac{\partial E}{\partial T} - \frac{1}{E}\frac{\partial \nu}{\partial T}\right)\sigma_{kk}\right)\dot{\sigma}_{kk} + \left(\frac{(1+\nu)}{E^2}\frac{\partial E}{\partial T} - \frac{1}{E}\frac{\partial \nu}{\partial T}\right)\sigma_{ij}\dot{\sigma}_{ij}\right\} \tag{8.41}$$

Equation (8.41) is known as the *revised version of the thermoelastic equation*, where the rate of temperature change is both a function of the stresses and their rate of change. It should be noted that C_p is used in Eq. (8.41). The higher order terms that constitute the difference between C_ε and C_p are neglected to allow Eq. (8.41) to be presented in a concise form. The difference between C_ε and C_p can be calculated using Eq. (8.8) and is negligible for most metals, and hence C_p is used here for consistency.

To illustrate more clearly the effects of the stresses in Eq. (8.41), a uniaxial stress system is considered, where $\sigma_{11} = \sigma_{kk}$ and $\sigma_{22} = \sigma_{33} = \sigma_{12} = \sigma_{23} = \sigma_{13} = 0$. Under these conditions, Eq. (8.41) can be written as follows [27]:

$$\dot{T} = -\frac{T_0}{\rho C_p}\left(\alpha - \frac{1}{E^2}\frac{\mathrm{d}E}{\mathrm{d}T}\sigma_{11}\right)\dot{\sigma}_{11} \tag{8.42}$$

Equation (8.42) shows that, for the revised treatment, the rate of temperature change is a function of the applied stress and its rate of change. It is now possible to integrate Eq. (8.42) over the time period corresponding to the deformation in a similar manner to the approach with Eq. (8.9). However, in a simple deformation process it is difficult to see what value should be used for the σ_{11}, that is, a static stress, which is independent of time. In a cyclic load, as with that used in TSA, σ_{11} could be regarded as the mean stress of the cycle σ_m, as this does not vary with time, and therefore Eq. (8.42) can be integrated to give

$$\Delta T = -\frac{T_0}{\rho C_\varepsilon}\left(\alpha - \frac{1}{E^2}\frac{\mathrm{d}E}{\mathrm{d}T}\sigma_m\right)\Delta\sigma_{11} \tag{8.43}$$

so that

$$\Delta T = -K^*\Delta\sigma_{11} \tag{8.44}$$

where K^* is the revised version of the thermoelastic constant, which is a function of the Young's modulus and the mean stress and can be written as

$$K^* = \frac{1}{\rho C_p}\left(\alpha - \frac{1}{E^2}\frac{\mathrm{d}E}{\mathrm{d}T}\sigma_m\right) \tag{8.45}$$

Equation (8.45) provides an expression for the thermoelastic constant that takes the stress dependence of α into account by incorporating the quantity $(1/E^2)\mathrm{d}E/\mathrm{d}T$ (Eq. (8.43)) and the σ_m term. If the material's Young's modulus is high and the $\mathrm{d}E/\mathrm{d}T$ term is small, then the mean stress will have a negligible effect on the thermoelastic response. The stress dependence of the thermoelastic constant for

Table 8.1 Material properties for three high-strength alloys.

Material	E (MPa)	dE/dT (MPa K^{-1})	σ_y (MPa)
4340 steel	210×10^3	−56.7	304
Al-2024	72×10^3	−36.0	197
Ti–6Al–4V	120×10^3	−61.8	430

a variety of materials is given in Table 8.1. The percentage difference between K^* values calculated at zero stress and at the yield stress was evaluated for each material. The greatest dependence (40%) was calculated for Ti–6Al–4V, with values of 10 and 14% obtained for Al-2024 and 4340 steel, respectively. Analysis of the material properties given in Table 8.1 shows that relative to the other materials Ti–6Al–4V has a relatively low E value combined with a high dE/dT and yield strength values.

Tutorial Exercise 8.3

It is known that the aluminum alloy used in Tutorial Exercise 8.1 has a dE/dT value of 0.7×10^{-4} MPa K^{-1}. Assuming uniaxial conditions, discuss how this will influence the TSA data.

Solution:

From Eq. (8.45)

$$\Delta T = -\frac{T_0}{\rho C_\varepsilon}\left(\alpha - \frac{1}{E^2}\frac{dE}{dT}\sigma_m\right)\Delta\sigma$$

The worst case scenario is that $\sigma_m = (\Delta(\sigma_1 + \sigma_2)/2)65$ MPa. The error in ΔT by neglecting the effect of σ_m is

$$\left(\frac{\Delta(\sigma_1+\sigma_2)}{2}\frac{1}{\alpha E^2}\frac{dE}{dT}\sigma_m\right) = 65 \times \frac{1}{23.5 \times 10^6 \times 60} \times 0.7 \times 10^{-4} = 0.05 \text{ or } = 5\%$$

The practical significance of the mean stress effect for the materials given in Table 8.1 can be established by calculating the percentage of the material's yield stress required to introduce an error of 5% by neglecting the mean stress dependence. Calculations were carried out for steel, an aluminum alloy, and a titanium alloy, with values of 29, 17, and 5% obtained, respectively. In practical terms, this analysis shows that, at least in the case of steel and aluminum, the mean stress effect will be effectively hidden within the ambient noise of the measurements (approximately 5%). The effect is shown to be significant in the case of the titanium alloys where a mean stress that is just 5% of the yield stress is required to introduce an error of 5% in the thermoelastic measurements. It has been shown that for nickel–titanium alloys (shape memory alloys) the effect can be

significant depending on the heat treatment the material has received this rendered quantitative analysis impossible because of the coupling of the mean stress and the stress change in Eq. (8.41).

It has been suggested [26] that the mean stress effect can be used to detect residual stresses. As residual stress is essentially a mean stress, it is accepted that the linear form of the TSA relationship given in Eq. (8.9) does not allow its evaluation. As described above, the changes in the thermoelastic response resulting from the inclusion of residual stress produce temperature change differences of a few millikelvin, which are significantly less than those expected to be resolved in standard TSA. At present, three approaches have been investigated as potential candidates for residual stress measurement using the thermoelastic response. Two are based on the mean stress effect and the revised higher order thermoelastic effect [26]. One utilizes the thermoelastic response at the second harmonic of the loading frequency [29], and the other directly relates the change in the thermoelastic response to the principal stresses [30]. The major limitation of these two approaches is that they are not suitable for steel components since the temperature dependence of the elastic properties of steel is negligible at room temperature. The third approach [31] is based on Eq. (8.9) and the change in the thermoelastic constant K resulting from plastic deformation during manufacture or assembly. In the third approach, the main disadvantage is that plastic deformation must have taken place, but it has the advantage that it may be valid for a larger range of materials, not just those with temperature-dependent elastic properties. A significant disadvantage common to all three approaches is that any change in the thermoelastic response resulting from either the mean stress σ_m or from the modification of K will be small. In actual components, the changes in the response are around the noise threshold of the detectors. Success in detecting these changes has been achieved by applying very large residual stress or plastic strain, by using materials that are very sensitive to the mean stress effect, or from investigation of specifically designed specimens. Recently, the sensitivity of infrared detectors has improved to the extent where it may be possible to accurately measure changes representative of those in actual components, thereby leading to a renewed interest using TSA for residual stress analysis. Since the variations in thermoelastic response are small, it is important to minimize sources of signal attenuation and to understand the possible sources of error within the measurement. The major factors known to influence the change in thermoelastic response (and subsequently K) are the high-emissivity coating, background temperature, applied stress, and the infrared detector settings; these effects must always be considered in parallel to any evaluations of the significance of changes in response due to mean stress or from the modification to K.

8.10
Progress, Applications, and Prospects

In 1990, TSA was the subject of a book edited by Harwood and Cummings [32]. It captured the then state of the art and covered aspects such as the mean stress effect,

applications to composite materials, paint coatings, and nonadiabatic behavior. It is an excellent publication, and most of the material is relevant today. Following on from this, there have been two good review papers: one in 1998 [33] that covered the development and applications on the technique, and another in 2001 [34] that brought together the theory for isotropic materials. In 2008, a special issue of the *Journal of Strain Analysis* (Vol. 43, No. 6), edited by the author, was published on the topic, which demonstrated the range of diversity of applications of TSA.

One of the most focused applications has been on crack-tip stress studies, with the intention of deriving the stress intensity factors (SIFs) from thermoelastic data alone (see, for example, [35–41]). The original treatment was based on the first-order Westergaard equations [35, 36], or equivalently, the singular terms in the eigenfunction expansion of Williams. This was demonstrated in [36], where the SIFs were obtained for simulated cracks (in the form of spark eroded slots) in mode I and mixed mode opening. The analysis in [36] made use of the cardioid geometry of the isopachics by deriving expressions for the SIFs in terms of the cardioid area and the positions of certain tangents to the curve. This treatment was fully exploited by developing algorithms and software that automatically obtained the SIFs from the thermoelastic data and demonstrated that the technique could be applied to actual cracks. Others have developed successful techniques for crack-tip stress studies, for example, [37, 38], based on the Mushkelishvili stress function. Recent work [39] directly fitted the cardioid form to extracted isopachics to estimate the crack-tip SIFs. The fitting was performed using a genetic algorithm (GA). An added advantage of the approach is that the crack tip is located in the data field, which can be difficult to detect by visual inspection. The technique has been applied to fatigue crack growth [40]. Most recently, attempts have been made to derive the higher order terms in the Westergaard equations [41]. The work is continuing, and the prospect of deriving very accurate SIFs from growing cracks in real structure is a distinct future possibility.

It is evident from Eq. (8.9) that, in the general case, the individual surface stress components cannot be directly derived from the thermoelastic response, and, consequently, the development of a means of determining individual surface stresses from the stress sum data, that is, stress separation, has become a topic of considerable importance. Work on stress separation, principally numerical, up to the mid-1990s is reviewed in [42]. Further studies over the last decade include hybrid photoelastic–thermoelastic techniques [43, 44] and other numerical approaches based on finite difference [45, 46] and finite element techniques [47]. It may be surmised that the additional effort and cost involved in implementing any one of these proposed approaches may be considerable. In [42], an approach is described that does not rely on the use of other techniques or additional computational effort but is based on the use of devices referred to as *thermoelastic strain gauges*. These can be bonded to the surface of a stressed specimen to provide a supplementary thermoelastic signal; from this signal and that from the adjacent surface of the specimen, individual stresses at the gauge position on the specimen surface can be derived. Clearly, the benefit of being able to deliver individual stresses from TSA is

clear. However, Eq. (8.9) provides a very important stress metric that can provide the basis for validation of numerical studies or the assessment of damage.

TSA has been applied extensively to composite materials, and some examples have been given earlier in the chapter. Studies relating to stress analysis of composite structure are few. An example for aircraft sandwich structures is given in [48]. Growth areas are high-resolution studies, damage assessments, and evaluation of stress in complex components and assemblies. Residual stress assessment using TSA is a topic of current interest, and with the growth of more sensitive detectors this is becoming a real possibility. However, the major bar to progress is the need for a cyclic load. Recent work [18] has shown that for composite materials it is possible to obtain quantitative data from a component subjected to a transient load. This represents a real step forward in progress and opens the technique for exploitation as a nondestructive examination (NDE) methodology.

Acknowledgments

The author would like to acknowledge the support of her coworkers and students in the production of this chapter, in particular Dr Trystan Emery and Dr James Eaton-Evans. She is extremely grateful to her former Ph.D. supervisor and coworker Emeritus Professor Peter Stanley from the University of Manchester, who introduced her to the technique and provided unrelenting encouragement to build on the research conducted in the early 1990s in a small laboratory in Manchester.

Problems

8.1 A further validation of the K value of Tutorial Exercise 8.2 is carried out at different frequencies. At 15 Hz, ΔT is obtained as 178 $\pm$0.006 K and at 30 Hz, ΔT150 $\pm$ 0.010 K. Explain the cause of the reduction in the response and devise a means of verifying K.

8.2 Describe the procedure and derive the equations to obtain K using a two-gauge orthogonal strain gauge rosette bonded to the component under investigation.

8.3 If the component in Tutorial Exercise 8.1 was made for Al-2024, explain how this would modify the influence of the mean stress value.

8.4 Is it possible to obtain residual stresses from TSA (i) using Eq. (8.12) and (ii) using Eq. (8.43). Describe an experiment procedure using only TSA to determine the material's sensitivity to the mean stress.

8.5 Explain why it is necessary to use imaging systems based on photon detectors for TSA.

8.6 In determining the sensitivity of a photon detector, why is it not sufficient to apply the standard Stefan–Boltzman relationship.

8.7 Explain how a Brazilian disc may be used to calibrate the thermoelastic response (see [9]).

8.8 Explain why in the vicinity of cracks and stress concentrations the thermoelastic response may not give an accurate representation of the stress field.

8.9 The image and plot shown below are obtained from a crack in an aluminum alloy plate loaded in uniaxial tension in the vertical direction. The plot shows ΔT and the phase. Explain why there is a step change in phase to the left of the plot and why there is an increase in phase to the right of the plot, in the vicinity of the crack tip.